Inorganic Chemistry

ARTICLE

pubs.acs.org/IC

Modeling the Geometric, Electronic, and Redox Properties of Iron(III)-Containing Amphiphiles with Asymmetric [NN′O] Headgroups

Rajendra Shakya,[†] Marco M. Allard,[†] Mara Johann,[‡] Mary Jane Heeg,[†] Eva Rentschler,[‡] Jason M. Shearer,[§] Bruce McGarvey,[∥] and Cláudio N. Verani*[,†]

[†]Department of Chemistry, Wayne State University, 5101 Cass Avenue, Detroit, Michigan 48202, United States

[‡]Institute of Inorganic and Analytical Chemistry, Johannes Gutenberg University, Duesbergweg 10-14 Mainz, 55128, Germany

[§]Department of Chemistry, University of Nevada, Reno, Nevada 89557, United States

[∥]Department of Chemistry and Biochemistry, University of Windsor, 401 Sunset Ave., Windsor, ON N9B 1P4, Canada

Supporting Information

ABSTRACT: Two iron(III)-containing amphiphiles **1** and **2** have been synthesized with the [NN′O] ligands $HL^{tBu\text{-}ODA}$ (2-((octadecyl(pyridin-2-ylmethyl)amino)methyl)-4,6-di-*tert*-butylphenol) and $HL^{I\text{-}ODA}$ (2-((octadecyl(pyridin-2-ylmethyl)amino)methyl)-4,6-diiodophenol), respectively. Compound **1** is monometallic, whereas EXAFS data suggest that **2** is a mixture of mono- and bimetallic species. The archetypical $[Fe^{III}(L^{NN'O})_2]^+$ complexes **3**−**9** have been isolated and characterized in order to understand the geometric, electronic, and redox properties of the amphiphiles. Preference for a monometallic or bimetallic nuclearity is dependent on (i) the nature of the solvent used for synthesis and (ii) the type of the substituent in the phenol moiety. In methanol, the *tert*-butyl-, methoxy-, and chloro-substituted **3**, **4**, and **5** are monometallic species, whereas the bromo- and iodo-substituted **6** and **7** form bimetallic complexes taking advantage of stabilizing methoxo bridges generated by solvent deprotonation. In dichloromethane, the bromo- and iodo-substituted **8** and **9** are monometallic species; however, these species favor meridional coordination in opposition to the facial coordination observed for the *tert*-butyl- and methoxy-substituted compounds. Molecular structures for species **5**, **7**, **8**, and **9** have been solved by X-ray diffraction.

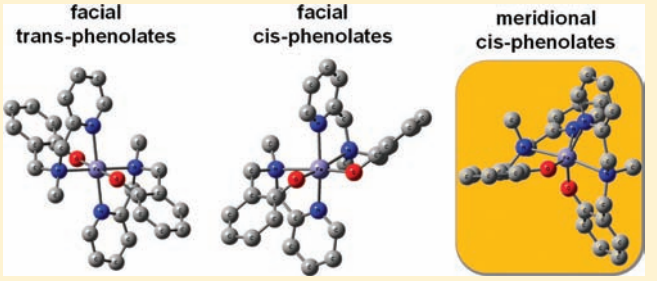

Furthermore, the electronic spectrum of the amphiphile **1** was expected to be similar to those of facial/cis archetypes with similar substituents, but close resemblance was observed with the profile for those meridional/cis species, suggesting a similar coordination mode. This trend is discussed based on DFT calculations, where preference for the meridional/cis coordination mode appears related to the presence of tertiary amine nitrogen on the ligand, as when a long alkyl chain is attached to the [NN′O] headgroup.

INTRODUCTION

Following previous results from our group, a research program has been established to study responsive metal-containing amphiphiles. Coordination and protonation preferences were studied on several amphiphiles. Of particular interest are $[ML_2]$ and $[ML_2]^+$ species containing cobalt,[1] nickel, copper, and zinc[2] ions coordinated to asymmetric NN′O chelating headgroups, due to their potential use in redox-responsive Langmuir−Blodgett films. Similar ligands have been investigated with several different metal centers,[3] and both structural and electronic effects play a role in determining the preferential geometry adopted by the resulting complexes.

When equivalent asymmetric NN′O amines and imines are compared, structural rigidity of the ligand takes precedence to the electronic configuration of the metal ion and favors meridional coordination. On the other hand, electronic configuration prevails when flexible amines are involved; a facial coordination mode is preferred, and the metal dictates the preferential cis or trans orientation of equivalent phenolates, pyridines, and amines in vicinal ligands. It has been observed that ions with a $3d^5$ high-spin configuration, such as trivalent iron, led to cis-arrangements of the phenols, whereas ions with $3d^6$ low-spin and $3d^7$ high-spin configurations, such as trivalent and bivalent cobalt, seem to support trans orientation of the phenols. Ions with a $3d^{10}$ configuration, such as bivalent zinc or trivalent gallium, do not seem to exhibit a clear preference because they lack any ligand field stabilization energy. These observations are guiding the design of metal-containing amphiphiles as precursors for redox-responsive films.

Because of superior redox-reversibility, iron compounds are of particular relevance; however, during the development of studies with iron-based amphiphiles, some discrepancies were observed. Complexes containing *tert*-butyl and iodo substituents on the phenol ring of the ligands $(L^{tBu\text{-}ODA})^-$ and $(L^{I\text{-}ODA})^-$ shown in Scheme 1 seemed to yield inconsistent behavior with the

Received: May 4, 2011
Published: August 01, 2011

Scheme 1. Amphiphilic and Archetypical Iron(III) Complexes

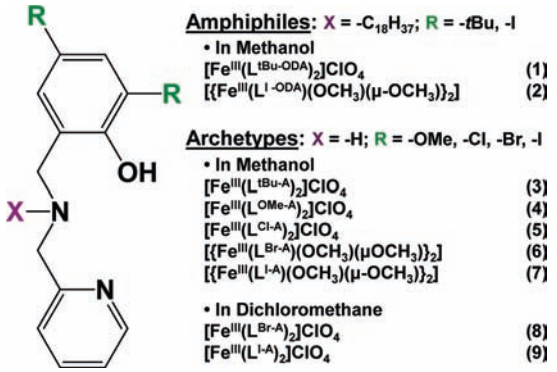

Scheme 2. Anticipated Amphiphilic Species

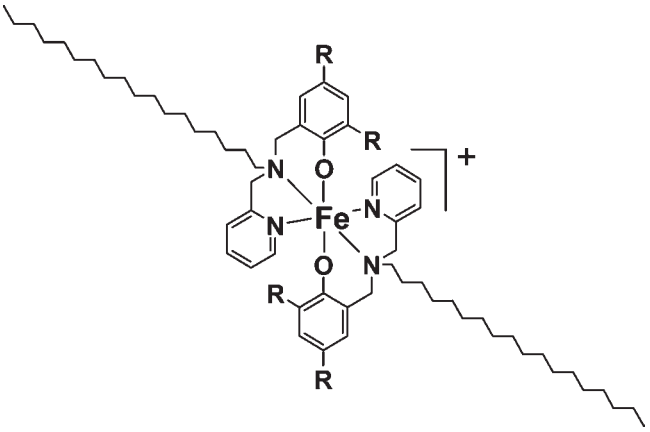

expected observations for archetypical iron(III) compounds with similar substituents.[4] This prompted us to assess these observations in deeper detail, and in this paper, we have developed a series of discrete mono- and binuclear iron-containing archetypical complexes. These species contain the NN′O chelating headgroup present in the amphiphiles, but omit the hydrophobic alkyl chain, and were studied in terms of their geometric and structural preferences as a function of (i) the ligand substituent and (ii) the role played by the solvent.

We have characterized these species thoroughly using several spectrometric, spectroscopic, electrochemical, and structural methods and comparing with computational models. These results follow and are expected to serve as guidelines for the synthesis of metal-containing amphiphiles.

RESULTS AND DISCUSSION

Anticipated Amphiphilic Products. From our previous results, we observed that cobalt compounds containing *tert*-butyl or chloro substituents occupying the third and fifth positions of the phenol ring show reversible ligand-centered processes in their electrochemical behavior.[1] We also observed that, due to their higher polarizability, the iodo-substituted amphiphilic ligand $HL^{I\text{-}ODA}$ shows enhanced amphiphilicity in the metal complexes.[5] In this study, we used the ligands $HL^{tBu\text{-}ODA}$ and

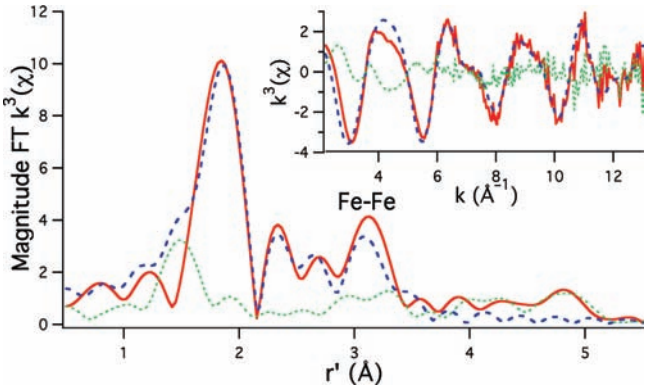

Figure 1. Magnitude FT k^3 EXAFS data and unfiltered k^3 EXAFS data (inset) for **2**. The experimental data are given as the red solid line, the best fit to the EXAFS data is given as the blue dashed line, and the difference spectrum is given as the dotted green line. Best fit for **2** included the following. Shell #1 (N/O shell): n = 4 (restrained), r = 1.891(3) Å, and σ^2 = 0.0031(4) Å^2. Shell #2 (N/O shell): n = 2 (restrained), r = 2.121(7) Å, and σ^2 = 0.0058(10) Å^2. Shell #3 (Fe shell): n = 0.6(1), r = 3.008(6) Å, and σ^2 = 0.002(1) Å^2. Shell #4 (C shell): n = 3.4(2), r = 2.53(1) Å, and σ^2 = 0.008(3) Å^2. E_o = 7120.2 eV; pre-edge peak, E = 7113.5(1) eV; area = 0.13(2) eV (relative to the edge); ε^2 = 0.93.

$HL^{I\text{-}ODA}$ for the development of iron-containing amphiphiles **1** and **2**, respectively. These were expected to display a better balance between electrochemical and amphiphilic properties, leading to superior precursors for LB films. The ligands were obtained as reported[2,4] and were thoroughly characterized. Upon treatment with iron(III) perchlorate in the presence of base in MeOH, intense purple-colored products of a waxy texture were isolated. According to our previous results,[4] the formation of the monomeric species $[Fe^{III}(L^{tBu\text{-}ODA})_2]^+$ and $[Fe^{III}(L^{I\text{-}ODA})_2]^+$ was anticipated (Scheme 2).

However, these complexes showed unexpected IR features, and along with C−H stretches associated with the octadecyl group; only $[Fe^{III}(L^{tBu\text{-}ODA})_2]ClO_4$ (**1**) displayed a prominent peak at ∼1098 cm^{-1} associated with the perchlorate counterion. The ESI$^+$ mass analysis for **1** showed a multi-isotopic distribution pattern related to iron (i.e., ^{54}Fe 5.8%, ^{56}Fe 91.7%, ^{57}Fe 2.2%, ^{58}Fe 0.3%), and C, H, N, O isotopes. The peaks at m/z = 1210.9 for the monomeric cation $[Fe(L^{tBu\text{-}ODA})_2]^+$and 579.3 for $[L^{tBu\text{-}ODA}]^+$ predominated, indicating the presence of a monomeric species in solution. Similarly, the ESI$^+$ mass spectrum for **2** presents a peak at m/z = 1489.7 for $[Fe^{III}(L^{I\text{-}ODA})_2]^+$. However, two other peaks with similar isotopic distribution are observed at m/z = 1638.6 and m/z = 1593.2 and indicate the presence of a dimeric product. Additionally, a considerable difference was observed between the UV−visible spectrum of **1** and that of the previously published[4] monomeric $[Fe(L^{tBuA})_2]ClO_4$ (**3**). Moreover, the electronic spectrum of **2** differed considerably from that of **1**.

In an effort to understand the reasons for such differences, species **2** was analyzed by X-ray absorption spectroscopy. A small Fe(1s → 3d) transition is observed at 7113.5(1) eV with a peak area of 0.13 eV (relative to the edge height). This is consistent with iron contained in a centrosymmetric (i.e., six-coordinate) ligand environment.[6] The resulting EXAFS data are shown in Figure 1 and in Figure S1 (Supporting Information) and is best modeled with iron(III) in an average $(N/O)_6$ coordination

dx.doi.org/10.1021/ic2009368 |*Inorg. Chem.* 2011, 50, 8356–8366

Scheme 3. Structure of the Dimeric Archetypes 6 and 7

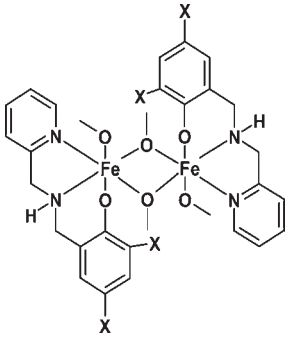

environment with one long Fe−(N/O) shell containing two scatterers at 2.12 Å and one shorter shell containing four Fe−(N/O) scatterers at 1.89 Å. A well-ordered outer-sphere Fe−Fe shell was also located at 3.01 Å. A best fit to the EXAFS data for this Fe−Fe shell yields 0.6(1) iron scatterers per complex. Although determining the number of scatterers by EXAFS is a difficult task, attempts to model this feature as multiple scatterings or other outersphere scatterers were unsuccessful. Therefore, it is reasonable to suggest that species **2** is composed of ca. 50−75% of an Fe−Fe dimer, while the remaining 25−50% is monomeric in nature.

To gather further electronic and structural information pertinent to **1** and **2**, we investigated the iron complexes **3**−**9** with archetypical ligands HL^{RA}, where R = *tert*-butyl, methoxy, chloro, bromo, and iodo phenol substituents.

Synthesis and Characterization of the Archetypical Complexes. *Monomeric Archetypes **3**, **4**, and **5** in Methanol.* Archetypical *tert*-butyl-, methoxy- and chloro-substituted complexes $[Fe^{III}(L^{tBu\text{-}A})_2]ClO_4$ (**3**), $[Fe^{III}(L^{OMe\text{-}A})_2]ClO_4$ (**4**), and $[Fe^{III}(L^{Cl\text{-}A})_2]ClO_4$ (**5**·MeOH) were synthesized by treatment of the corresponding protonated ligands $HL^{tBu\text{-}A}$, $HL^{OMe\text{-}A}$, and $HL^{Cl\text{-}A}$ with hydrated ferric perchlorate in the presence of a base to support phenol deprotonation. The IR features coincide with those described above for the amphiphilic **1**, and ESI^+ mass analysis showed a prevalent m/z peak consistent with each respective and expected $[ML_2]^+$ species.

*Dimeric Archetypes **6** and **7** in Methanol.* Aiming at other $[Fe^{III}(L)_2]^+$ complexes with bromo and iodo substituents on the phenol ring, reactions were carried out with ligands $HL^{Br\text{-}A}$ and $HL^{I\text{-}A}$. Microcrystalline samples were isolated, and their IR spectra showed an absence of peaks associated with the perchlorate counterion. The ESI^+ mass spectrometry showed a distinct profile dissimilar to that observed for **3**, **4**, and **5**, but fitting the description of a dimer described as $[\{Fe^{III}(L^{R\text{-}A})(OCH_3)(\mu\text{-}OCH_3)\}_2]$ (R = -Br for **6** and -I for **7**), and shown in Scheme 3. Use of a 1:1 ligand-to-metal stoichiometry led to similar results, and recrystallization in methanol gave dark-colored diffraction-grade crystals for **6** and **7**.

*Monomeric Archetypes **8** and **9**·CH_2Cl_2·H_2O in Dichloromethane.* The dimeric **6** and **7** show that methoxy groups act as bridges between two $[LFe]^{2+}$ units. These bridges are likely originated from MeOH, and therefore, one can conclude that the absence of the solvent would lead to the formation of monomeric $[FeL_2]^+$ species. Consequently, reactions in dichloromethane were performed in a 2:1 ligand-to-iron ratio. Indeed, the dark-colored microcrystalline $[Fe^{III}(L^{Br\text{-}A})_2]ClO_4$ (**8**) and

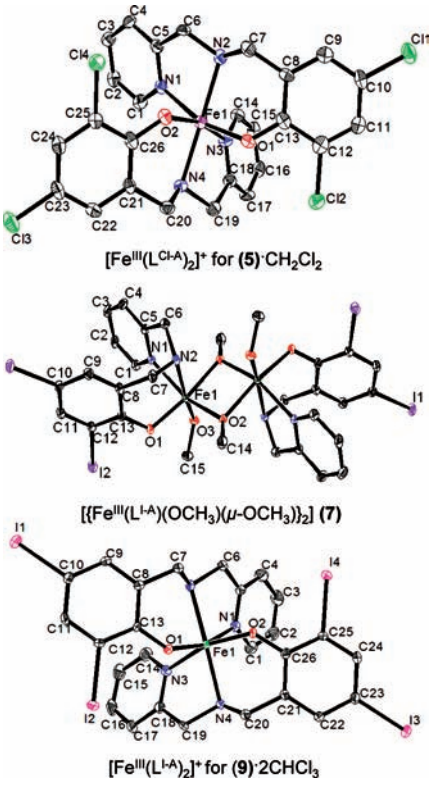

Figure 2. ORTEP representations for the cation of **5**·CH_2Cl_2, **7**, and the cation of **9**·2$CHCl_3$.

$[Fe^{III}(L^{I\text{-}A})_2]ClO_4$ (**9**·CH_2Cl_2·H_2O) were isolated and their IR spectra showed intense peaks at ∼1090 cm^{-1} attributed to the perchlorate counterion. This is in good agreement with the observed results for **1** and **2**. Accordingly, the ESI^+ mass analysis showed m/z peaks exclusively related to the $[ML_2]^+$ fragment.

Molecular Structures. Upon crystallization in MeOH/CH_2Cl_2 and in MeOH/$CHCl_3$, respectively, **5**·MeOH and **9**·CH_2Cl_2·H_2O yielded X-ray quality crystals described as **5**·CH_2Cl_2 and **9**·2$CHCl_3$. Compounds **6** and **7** yielded crystals from their methanol mother solutions. These species had their structures determined. Representative ORTEP plots for **5**·CH_2Cl_2, **7**, and **9**·2$CHCl_3$ are presented in Figure 2. The structure for **6** is shown in Figure S2 (Supporting Information). Selected bond lengths and bond angles are shown in Table 1.

*$[Fe^{III}(L^{Cl\text{-}A})_2]ClO_4$ (**5**·CH_2Cl_2) and $[Fe^{III}(L^{I\text{-}A})_2]ClO_4$ (**9**·2$CHCl_3$).* Both structures consist of discrete mononuclear molecules. An iron(III) ion is coordinated to two deprotonated ligands in a pseudo-octahedral environment via the pyridine and amine nitrogen and phenolate oxygen atoms of each ligand. Species **5**·CH_2Cl_2 and **9**·2$CHCl_3$ display a meridional arrangement of each of the tridentate NN′O ligands. Interestingly, comparison between **5**·CH_2Cl_2, **9**·2$CHCl_3$, and the previously published **3** shows the ligands facially coordinated in the latter species. This result reinforces the notion that mer and fac isomers are separated by a small energy difference calculated to be 2.4 kcal/mol. Furthermore, t he arrangement of the donors in **5**·CH_2Cl_2 and **9**·2$CHCl_3$ is $[Fe<N_{am1}N_{am2}><N_{py1}O_{phO1}><N_{py2}O_{PhO2}>]$[7] with two pyridines and two phenolates cis-arranged to each other, rather than the observed $[Fe<N_{am1}O_{PhO2}><N_{am2}O_{phO1}><N_{py1}N_{py2}>]$ for **3**. The meridional coordination modes of **5**·CH_2Cl_2 and **9**·2$CHCl_3$ are comparable to that of the imine complex $[Fe^{III}(L^{tBu\text{-}I})_2]ClO_4$.[4] In

dx.doi.org/10.1021/ic2009368 |*Inorg. Chem.* 2011, 50, 8356–8366

Table 1. Selected Bond Distances (Å) and Angles (°) for $5\cdot CH_2Cl_2$, 6, 7, and $9\cdot 2CHCl_3$

$5\cdot CH_2Cl_2$	6	7	$9\cdot 2CHCl_3$
Fe(1)−O(1) 1.900(3)	Fe(1)−O(1) 1.958(3)	Fe(1)−O(1) 1.9607(14)	Fe(1)−O(1) 1.916(4)
Fe(1)−O(2) 1.914(3)	Fe(1)−O(4) 2.030(3)	Fe(1)−O(2) 1.9758(14)	Fe(1)−O(2) 1.909(4)
Fe(1)−N(4) 2.146(4)	Fe(1)−O(4)′ 1.970(3)	Fe(1)−O(2)′ 2.0365(14)	Fe(1)−N(4) 2.156(4)
Fe(1)−N(2) 2.146(4)	Fe(1)−N(1) 2.255(4)	Fe(1)−N(1) 2.1543(17)	Fe(1)−N(2) 2.150(5)
Fe(1)−N(1) 2.170(4)	Fe(1)−N(2) 2.156(3)	Fe(1)−N(2) 2.2649(18)	Fe(1)−N(1) 2.181(5)
Fe(1)−N(3) 2.172(4)	Fe(1)−O(3) 1.902(3)	Fe(1)−O(3) 1.8977(15)	Fe(1)−N(3) 2.170(5)
O(1)−Fe(1)−O(2) 97.39(12)	O(3)−Fe(1)−O(1) 99.58(11)	O(3)−Fe(1)−O(1) 101.07(6)	O(1)−Fe(1)−O(2) 101.38(17)
O(1)−Fe(1)−N(4) 92.41(14)	O(3)−Fe(1)−O(4) 91.67(11)	O(3)−Fe(1)−O(2) 98.12(6)	O(1)−Fe(1)−N(4) 93.29(16)
O(2)−Fe(1)−N(4) 90.06(14)	O(1)−Fe(1)−O(4) 168.73(11)	O(1)−Fe(1)−O(2) 99.55(6)	O(2)−Fe(1)−N(4) 89.66(16)
O(1)−Fe(1)−N(2) 89.94(13)	O(3)−Fe(1)−O(4)′ 98.27(12)	O(3)−Fe(1)−O(2)′ 91.10(6)	O(1)−Fe(1)−N(2) 88.90(16)
O(2)−Fe(1)−N(2) 91.79(14)	O(1)−Fe(1)−O(4)′ 99.01(11)	O(1)−Fe(1)−O(2)′ 167.73(6)	O(2)−Fe(1)−N(2) 93.68(16)
O(1)−Fe(1)−N(1) 162.91(14)	O(4)−Fe(1)−O(4)′ 79.83(11)	O(2)−Fe(1)−O(2)′ 80.04(6)	O(1)−Fe(1)−N(1) 163.13(17)
O(2)−Fe(1)−N(1) 91.23(12)	O(3)−Fe(1)−N(2) 97.15(12)	O(3)−Fe(1)−N(1) 97.07(7)	O(2)−Fe(1)−N(1) 86.96(17)
N(4)−Fe(1)−N(1) 102.34(15)	O(1)−Fe(1)−N(2) 89.85(12)	O(1)−Fe(1)−N(1) 89.80(6)	N(4)−Fe(1)−N(1) 101.46(17)
N(2)−Fe(1)−N(1) 75.02(14)	O(4)−Fe(1)−N(2) 88.11(11)	O(2)−Fe(1)−N(1) 160.26(6)	N(2)−Fe(1)−N(1) 75.84(17)
O(1)−Fe(1)−N(3) 91.36(13)	O(4)′−Fe(1)−N(2) 160.65(12)	O(2)′−Fe(1)−N(1) 87.14(6)	O(1)−Fe(1)−N(3) 88.80(17)
O(2)−Fe(1)−N(3) 163.08(14)	O(3)−Fe(1)−N(1) 170.05(12)	O(3)−Fe(1)−N(2) 169.58(7)	O(2)−Fe(1)−N(3) 162.29(17)
N(4)−Fe(1)−N(2) 176.80(14)	O(1)−Fe(1)−N(1) 87.28(12)	O(1)−Fe(1)−N(2) 86.58(6)	N(4)−Fe(1)−N(2) 175.57(17)
N(4)−Fe(1)−N(3) 75.06(14)	O(4)−Fe(1)−N(1) 81.48(11)	O(2)−Fe(1)−N(2) 87.46(6)	N(4)−Fe(1)−N(3) 75.18(17)
N(2)−Fe(1)−N(3) 102.72(15)	O(4)′−Fe(1)−N(1) 87.67(12)	O(2)′−Fe(1)−N(2) 81.16(6)	N(2)−Fe(1)−N(3) 101.04(18)
N(1)−Fe(1)−N(3) 84.28(13)	N(2)−Fe(1)−N(1) 75.52(12)	N(1)−Fe(1)−N(2) 75.70(7)	N(1)−Fe(1)−N(3) 87.15(18)

that report, we hypothesized that the imine ligand coordinates meridionally because of its rigidity, whereas the amines can accommodate facial coordination. The result described here suggests that meridional coordination modes also depend upon the nature of the substituents present in the phenol moiety. The average observed $Fe-O_{(PhO)}$ and $Fe-N_{am}$ bond distances of 1.906 and 2.146 Å, respectively, in $5\cdot CH_2Cl_2$ and 1.912 and 2.152 Å, respectively, in $9\cdot 2CHCl_3$ are in good agreement with literature values.[4,8] In both structures, one trans angle, N4−Fe1−N2, is very close to 180°, whereas the other two trans angles, O1−Fe1−N1 and O2−Fe1−N3, deviate by ∼17° from an ideal 180°. The N2−Fe1−N1 and N4−Fe1−N3 angles approach 75° and are within range for five-membered chelate rings.[8c]

*[{$Fe^{III}(L^{Br\text{-}A})(OCH_3)(\mu OCH_3)\}_2$] (**6**) and [{$Fe^{III}(L^{T\text{-}A})(OCH_3)(\mu$-$OCH_3)\}_2$] (**7**).* Both complexes crystallize as discrete molecules in the triclinic space group *P*1. In each case, the neutral species consists of two hexacoordinated iron(III) centers, both in a pseudo-octahedral environment, coordinated by N_2O_4-donor sets and related by a crystallographic inversion center. The ligands around each iron center are facially coordinated via an [NN′O] donor set from the pyridine, amine, and phenolate, respectively. The octahedral environment of each iron(III) center is completed by a single terminal methoxo ligand and a pair of μ-methoxo bridging ligands that connect the two metal ions. The coordination mode around each iron center is described as $[Fe<O_{phO1}O_{\mu\text{-}OMe2}><N_{am1}O_{OMe2}><N_{py1}O_{\mu\text{-}OMe1}>]$. The Fe_2O_2 core is asymmetric in both **6** and **7** due to distinctive $Fe-O_{\mu\text{-}OCH3}$ bond lengths (e.g., 2.037 and 1.975 Å in **7**). This rhombus-like motif is similar to that of other dimers reported in the literature.[9] This asymmetry can be explained by the structural trans effect.[10] The longer $Fe-O_{methoxy}$ bond of the Fe_2O_2 core lies trans to the shorter $Fe-O_{phenolate}$ bonds, whereas the shorter $Fe-O_{methoxy}$ bonds are trans to the longer $Fe-N_{pyridine}$ bond. The Fe−O−Fe angles are ca. 100° for both **6** and **7**, and consequently, the O−Fe−O angles are ca. 80°, thus leading the remaining angles around each iron center to be distorted from the ideal octahedron.[11,12]

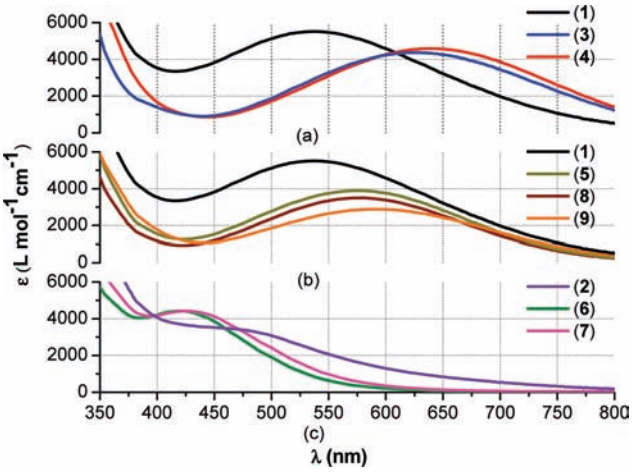

Figure 3. Selected UV−visible spectra in dichloromethane, 1.0×10^{-4} M: (a) **1**, **3**, and **4**; (b) **1**, **5**, **8**, and **9**; (c) **2**, **6**, and **7**.

Electronic Spectroscopy. The electronic behavior of the amphiphilic **1** and **2**, as well as of the archetypes **3**−**9**, was studied by UV−visible spectroscopy in dichloromethane. These spectra are shown in Figure 3a−c and summarized in Table 2. The amphiphile **1** exhibits two intense bands in the near-UV region (284 and 329 nm) and one band at 536 nm in the visible region. The ligand does not show absorption above 300 nm, and the intensities of the spin-forbidden d−d transitions for high-spin Fe^{III} complexes are expected to be irrelevant. Therefore, the bands at 329 and 536 nm are assigned to ligand-to-metal charge transfer (LMCT) processes. The low-energy band (536 nm) has

dx.doi.org/10.1021/ic2009368 |*Inorg. Chem.* 2011, 50, 8356–8366

Table 2. Selected UV-Visible Spectroscopic Data for 1−9

complex	λ (nm)/ε (L mol^{-1} cm^{-1})[a]
$[Fe^{III}(L^{tBu\text{-}ODA})_2]^+$ (**1**)	284 (21 370); 329 (10 800); 536 (5470)
$[Fe^{III}(L^{I\text{-}ODA})_2(OCH_3)(\mu\text{-}OCH_3)\}_2]$ (**2**)	296 (18 400); 477 (3370)
$[Fe^{III}(L^{tBu\text{-}A})_2]^+$ (**3**)	276sh (11 100); 336 (8000); 638 (4600)
$[Fe^{III}(L^{OMe\text{-}A})_2]^+$ (**4**)	278 (10 360); 326 (8030); 626 (4070)
$[Fe^{III}(L^{Cl\text{-}A})_2]^+$ (**5**)	295 (15 400); 331 (7820); 548 (3590)
$[\{Fe^{III}(L^{Br\text{-}A})(OCH_3)(\mu\text{-}OCH_3)\}_2]$ (**6**)	302 (17 400); 419 (5130)
$[\{Fe^{III}(L^{I\text{-}A})(OCH_3)(\mu\text{-}OCH_3)\}_2]$ (**7**)	298 (18 120); 426 (4930)
$[Fe^{III}(L^{Br\text{-}A})_2]^+$ (**8**)	298 (11 110); 332 (6700); 558 (3270)
$[Fe^{III}(L^{I\text{-}A})_2]^+$ (**9**)	(20 400); 339 (8230); 588 (3390)

[a] Spectra measured in CH_2Cl_2 for **1**−**9**. All solutions are 1.0×10^{-4} M in dichloromethane. All counterions are perchlorate.

Table 3. Electrochemical Parameters for Compounds 1−9

	metal-centered process	ligand-centered processes	
		reductions[a]	oxidations[b]
compounds	(V vs Fc^+/Fc)/(ΔE)	(V vs Fc^+/Fc)	(V vs Fc^+/Fc)
$[Fe^{III}(L^{tBu\text{-}ODA})_2]^+$ (**1**)	−0.83 (0.16)	+0.63, +0.22	+0.46, +0.74
$[Fe^{III}(L^{I\text{-}ODA})_2(OCH_3)(\mu\text{-}OCH_3)\}_2]$ (**2**)	−0.54 (0.13), −0.92 (0.11)	+0.77, +0.42, +0.07	+0.58, +1.13
$[Fe^{III}(L^{tBu\text{-}A})_2]^+$ (**3**)	−1.11 (0.12)	+0.61 (0.11), +0.93 (0.20)	
$[Fe^{III}(L^{OMe\text{-}A})_2]^+$ (**4**)	−0.82 (0.11)	+0.77, +0.32	+0.64, +0.95
$[Fe^{III}(L^{Cl\text{-}A})_2]^+$ (**5**)	−0.64 (0.16)	+1.02 (0.12)	
$[\{Fe^{III}(L^{Br\text{-}A})(OCH_3)\ (\mu\text{-}OCH_3)\}_2]$ (**6**)	−1.16 (0.05)	+0.98, +0.26	+1.05, +0.60
$[\{Fe^{III}(L^{I\text{-}A})(OCH_3)\ (\mu\text{-}OCH_3)\}_2]$ (**7**)	−1.13 (0.08)	+0.94, +0.46	+1.01, +0.52
$[Fe^{III}(L^{Br\text{-}A})_2]^+$ (**8**)	−0.58 (0.18)	+0.54, −0.00	+1.13, +1.30
$[Fe^{III}(L^{I\text{-}A})_2]^+$ (**9**)	−0.57 (0.15)	+0.52, −0.08	+1.05, +1.24

[a] The potential given in the ligand-centered process is the cathodic peak potential E_{pc} vs Fc^+/Fc. [b] The potential given in the ligand-centered process is the anodic peak potential E_{pa} vs Fc^+/Fc.

been assigned to a $p\pi_{phenolate} \rightarrow d\pi^*_{iron}$ CT transition, whereas the band at higher energy (329 nm) is associated with the $p\pi_{phenolate} \rightarrow d\sigma^*_{iron}$ CT transition.[4,13] The UV−visible spectrum of the amphiphile **1** was expected to be similar to that of the archetype **3** where the iron center is described as $[Fe<N_{am1}O_{PhO2}><N_{am2}O_{phO1}><N_{py1}N_{py2}>]$. Although good overlap was observed for the bands at higher energy, considerable discrepancy was observed in the position of the low-energy band, implying that different coordination modes could be present in each of these complexes. These differences could arise from the relatively low energy difference between meridional and facial coordination of the [NN′O] ligands, previously calculated to be ∼3 kcal/mol for an iron-containing model with the unsubstituted ligand. The spectra of the new mononuclear archetypes **4**, **5**, **8**, and **9** were compared to those of **1** and **3** (Figure 3a−c). As expected, good overall agreement was observed between the *tert*-butyl-substituted **3** and the methoxy-substituted **4**, and the low-energy CT band appears within 630−640 nm (Figure 3a). One can infer that both species share a similar facial coordination mode. A different picture was observed for the chloro-, bromo-, and iodo-substituted **5**, **8**, and **9**, in which this CT band appears blue shifted to ca. 550−560 nm (Figure 3b). Comparatively, the behavior of the amphiphilic **1** fits well with that of **5**, **8**, and **9**, rather than with **3** and **4**, suggesting that its coordination mode should be similar to that of the former group.

Investigation of amphiphile **2** yielded shoulder-like features at 296 and 477 nm. This unusual profile was compared to the spectra of **6** and **7**. These dimeric complexes display bands at ca. 300 and 420 nm (Figure 3c). Similar to the spectra of monomeric complexes, the low-energy band is assigned to the $p\pi_{phenolate} \rightarrow d\pi^*_{iron}$ CT band, whereas the higher-energy band is associated with the $p\pi_{phenolate} \rightarrow d\sigma^*_{iron}$ transition. Additional contribution from the methoxy groups is also expected. Despite the similarities, significant blue shifting of the bands to 420−430 nm is observed for the dimeric species, when compared to the monomeric complexes. Among the probable reasons for this shifting, one can consider a weaker acidic character of the iron(III) ion in **6** and **7**. Furthermore, an increased electronic density at the metal can be caused by the presence of terminal and bridging electron-donating methoxo ligands.[14] However, **6** and **7** fail to mimic the ill-defined behavior observed for **2**, thus reinforcing the idea that this amphiphile entails the dimeric species along with a monomeric component, as revealed by EXAFS/XANES spectroscopy. These arguments are further investigated by DFT calculations.

Redox Properties. The redox behavior of the amphiphiles **1** and **2**, the monomeric complexes **3**−**5**·MeOH and **8**−**9**·CH_2Cl_2·H_2O, and the dimeric complexes **6** and **7** were studied by cyclic voltammetry (CV) in dichloromethane using $TBAPF_6$ as the supporting electrolyte. Redox potentials are given in Table 3, and selected CVs for **4**, **5**·MeOH, and **9**·CH_2Cl_2·H_2O are shown in Figure 4. For the amphiphile **1**, an ill-defined quasi-reversible metal-centered process is observed at ca. −0.83 V in dichloromethane vs Fc^+/Fc. The ligand-centered processes for this species were expected to mimic those of **3** with two reversible

dx.doi.org/10.1021/ic2009368 |*Inorg. Chem.* 2011, 50, 8356–8366

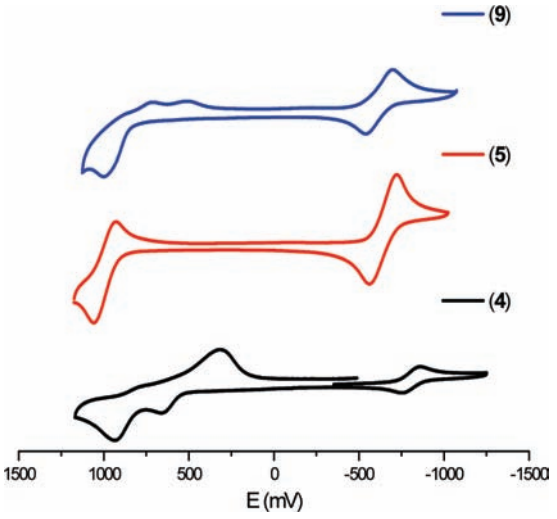

Figure 4. Cyclic voltammograms for **4**, **5**·MeOH, and **9**·$2CH_2Cl_2$·H_2O in 1.0 × 10^{-3} M dichloromethane, $TBAPF_6$ as supporting electrolyte.Values plotted vs Fc^+/Fc.

peaks for the phenolate/phenoxyl redox couple. Contrary to our expectation, irreversible ligand-centered oxidation peaks were observed at $E_{pa} \approx 0.22$ and 0.63 V vs Fc^+/Fc, along with the equivalent reductions at $E_{pc} \approx 0.46$ and 0.74 V vs Fc^+/Fc. This observation suggests that the reversible ligand-centered behavior of **3** associated with the *tert*-butyl groups is absent in **1**. This lack of reversibility is likely related to the modification of the amine group from secondary to tertiary upon incorporation of the octadecyl substituent. On the other hand, the amphiphile **2** presents an intricate ligand-centered redox behavior similar to that of the cobalt(II) complex with the same ligand.[1,4,5] For two observed oxidation processes (∼0.58 and 1.13 V vs Fc^+/Fc), three reduction peaks were observed (∼0.77, 0.42, 0.07 V vs Fc^+/Fc), suggesting the presence of multiple species in solution, either as a mixture or from follow-up reactions. The two quasi-reversible processes at −0.54 and −0.92 V vs Fc^+/Fc are attributed to the iron(III)/iron(II) redox couples. As will be seen, the former potential matches the expected value for the monomeric **9**, whereas the latter is well within that of the dimer **7**, further strengthening the idea that **2** is a mixture.

For the monomeric **4**, **5**·MeOH, **8**, and **9**·CH_2Cl_2·H_2O, the CVs show a fairly reversible metal-centered process consistent with that of **3**. The different potentials observed for this redox couple are attributed to the electronic effects of the phenol substituents, which are in good agreement with available Hammett parameters.[15] The ligand-centered processes differ considerably from those for **3**. The chloro-substituted **5**·MeOH displays one quasi-reversible process at 1.02 V vs Fc^+/Fc and reinforces our previous observation that chloro groups might be able to stabilize phenoxyl radicals.[1] Attempts to isolate a second ligand-centered process, as observed for **3**, led to ligand decomposition. Complexes **4**, **8**, and **9**·CH_2Cl_2·H_2O show irreversible and ill-defined oxidation and reduction peaks for the ligand-centered processes. This irreversibility is observed even when the second oxidation is excluded. Reversible metal-centered processes are observed for the dimeric **6** and **7** when the scan potentials are held within −1.0 and −1.4 V vs Fc^+/Fc. These peaks are significantly less intense than those for the monomeric species, indicating that considerable decomposition takes place during the redox process.

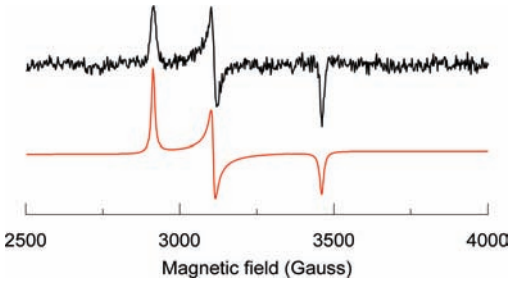

Figure 5. EPR spectrum of **9**·CH_2Cl_2·H_2O in dichloromethane glass at 118 K. The black trace is the experimental data, and the red trace is the simulated data. The *g* values are 2.31, 2.17, and 1.94.

EPR Spectroscopy. In an approximate octahedral field, the $3d^5$ iron(III) ion will show $S = 5/2$ in a high-spin configuration, whereas the low-spin case will lead to an $S = 1/2$. In a previous paper,[4] we have pointed out that the imine counterpart of **3**, but not **3** itself, displayed 5/2 ↔ 1/2 spin equilibrium in solution. On the basis of that observation, recent articles by Shongwe et al.[16] and Tang et al.[17] have investigated this effect in great detail, proposing a thermally induced $^6A_1 \leftrightarrow {}^2T_2$ two-step spin crossover for monomeric iron(III) complexes with similar NN′O ligands containing rigid C═N bonds. As previously proposed by Sim et al.,[18] such spin equilibria depend on the nature and position of the substituents in the phenolate ring. Aiming at a deeper evaluation of the electronic configuration of the monomeric amine species **4**, **5**, **8**, and **9**, EPR spectra were measured at 118 K in dichloromethane glass. All species show a similarly intense signal at $g \sim 4.3$, along with two or three less intense signals between $g \sim 6$ and 8. These peaks are expected with a predominant high-spin character, and the main peak at $g \sim 4.3$ occurs when the zero-field parameters *D* and *E* meet the criteria of $|D| \gg h\nu$ and $|E| \approx |D/3|$, thus supporting the expected behavior for such rhombic pseudo-octahedral species.[19] Although these spectra are fairly similar and unquestionably belong to an $S = 5/2$ spin scaffold, quantitative information for the less intense signals observed in **4**, **5**, **8**, and **9** using X-band spectrometers is a nontrivial pursuit. Besides *D* and *E*, each $S = 5/2$ spectrum has three other different and variable zero-field parameters, namely, B_4^0, B_4^2, and B_4^4. Moreover, the *D* values are larger than 1 cm^{-1}, and the *E* values are slightly smaller than *D*/3.[20] High magnetic fields would be required in order to understand the subtle differences between each compound.

For **3** and **4**, where the ligand is coordinated facially to the metal center, no other signal is detected at higher magnetic fields between 2500 and 4000 G. However, a low-intensity frozen liquid $S = 1/2$ spectrum is observed for **5**, **8**, and **9** with widely divergent *g* values of 2.31, 2.17, and 1.94. Figure 5 shows an illustrative example for complex **9**. The *g* values in each of these species is typical of a low-spin iron(III) system. The presence of the $S = 1/2$ species along with the expected predominant high-spin $S = 5/2$ species leads us to conclude that **5**, **8**, and **9** present some degree of spin admixture.

Except for a very distorted symmetry, the EPR signals from the high-spin Fe(III) site reveal little additional information. However, the *g* values for the low-spin site give considerable information about the lowest three spin states of Fe(III). In a strong ligand field of octahedral symmetry, the ground state consists of three t_2-like orbitals occupied by five electrons. The spin−orbit interaction splits the 6-fold degeneracy into three Kramer's

dx.doi.org/10.1021/ic2009368 |*Inorg. Chem.* 2011, 50, 8356–8366

doublets with one doublet lowest in energy and the other two doublets higher by λ, the spin−orbit constant. The three g values for the ground-state doublet are 2.00. The EPR for the octahedral system is only observed at liquid He temperatures. For ligand field distortions larger in magnitude than λ, the g values for the ground state doublet diverge greatly from 2.00 and the EPR is readily detectable at liquid nitrogen temperatures. The theoretical treatment of this system is available in recent reviews[21] and allows us to extract three parameters from the g values: the orbital reduction factor for covalency K and the energy parameters Δ and V. The energy parameters need careful definition, because what is important is the difference in energy between the highest and lowest state and where the middle energy level is in reference to the top and bottom levels. We start by defining the energies of the three t_2-like orbitals as E_x, E_y, and E_z. The subscript refers to the axis perpendicular to the plane of the molecular orbital.[22] The energies are the ligand field energies before electrons are added, and the effect of the spin−orbit interaction can be calculated. Two parameters are then defined: $\Delta = [E_z - {}^1/_2(E_y - E_x)]/\lambda$ and $V = (E_y - E_x)/\lambda$. In applying the theory, the value of V is not allowed to be greater than $2\Delta/3$, which occurs when E_y is halfway between E_x and E_z. To allow for the case when E_z is less than the E_x and E_y, we allow Δ to be negative and V to go between 0 and $-2|\Delta|/3$. Note that the x,y,z coordinate system is defined in terms of the energy values and has nothing to do to with the symmetry of the molecular iron site. Failure to restrict the definition in this way leads to confusing multiple solutions. The sign of Δ can be obtained easily from the g values. If two g values are greater than 2.0 and one g value is smaller than 2.0, then Δ is positive and the smallest g is described as g_z. For the observed values of 2.31, 2.17, and 1.94, values of $K = 0.926$, $V = 3.94$, and $\Delta = 7.90$ can be calculated. An appropriate value for λ would be 107 cm^{-1}. The z direction in complex **9** can be estimated using the following reasoning. The three t_2-like orbitals contain planar d orbitals in three orthogonal planes that interact in a π fashion with the p orbitals of the ligand oriented in the same plane. Therefore, the three t_2-like orbitals belong to π antibonding MOs. Thus, before applying the spin−orbit interaction, the unpaired electron occupies the antibonding MO with the strongest π bonding; the spin−orbit interaction, however, tends to mix up the spins and MOs. It is most likely that the major π interaction occurs through $O_{phenolate}$ and $N_{pyridine}$ p orbitals oriented perpendicular to the plane of the aromatic ring to which they are bound. If the two rings in the ligand were exactly parallel, then the xy MO would π interact with both ligands, while the xz and yz MOs would only interact with one ligand. This would result in $\Delta > 0$ and $V = 0$. Because the rings are not parallel, V should be greater than zero. Thus, our best guess would be that the z direction must be perpendicular to the FeO_2 plane in the complex. These data suggest that—as relevant as the ligand rigidity—is the meridional coordination of the amine ligands around the iron(III) ion. When such a coordination mode is observed, a $5/2 \leftrightarrow 1/2$ spin admixture is detected. The extent to which spin crossover can be sustained in these flexible amine-based systems still needs to be determined.

Magnetic Susceptibility. Magnetic susceptibility data for polycrystalline samples of **6** and **7** were collected in the temperature range of 2−300 K. The spin Hamiltonian $H = -2JS_1 \cdot S_2$ with $S_1 = S_2 = 5/2$ was used for both compounds that show nearly identical antiferromagnetic behavior. Figure 6 displays the temperature-dependent measurement of the magnetic moment for **6** as the $\mu_{eff}(\mu_B)$ vs T(K) curve, whereas data for **7** are available in the Supporting Information (Figure S3). Results for **6** and **7** show an effective magnetic moment at 295 K of 7.58 μ_B for **6** and 7.49 μ_B for **7**, thus smaller than the theoretical value of 8.37 μ_B expected for two uncoupled iron(III) centers and indicative of coupling at room temperature. The effective magnetic moments of both compounds decrease as the temperature is lowered. The μ_{eff} values of 4.64 μ_B at 50 K, 1.97 μ_B at 10 K, 1.20 μ_B at 5 K, and 0.68 μ_B at 2 K for **6** (as well as 4.63, 2.00, 1.36, and 0.85 μ_B for **7**) indicate a diamagnetic ground state of $S_t = 0$ arising from antiparallel spin coupling between two high-spin iron(III) centers. Both species had their data simulated.

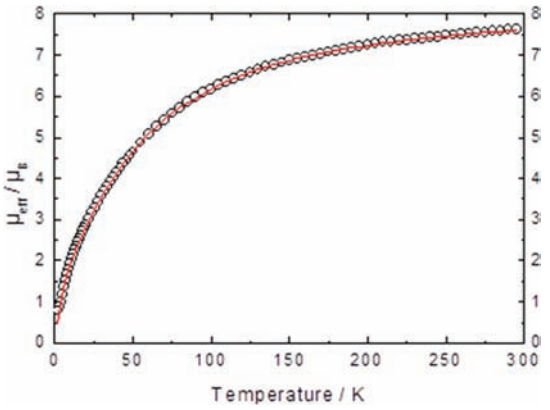

Figure 6. Temperature-dependent measurement of the magnetic moment for **6**. The experimental data are given as black circles, and the simulated curve is given by the red trace.

Table 4. Magnetic Data for Species 6 and 7

	6		7	
field	0.2 T	0.5 T	0.2 T	0.5 T
J (cm^{-1})	−5.97	−6.02	−6.01	−6.02
g	2.00	2.00	2.00	2.00
θ_{Weiss} (K)	−2.2	−3.5	−11.9	−12.4

Table 4 displays the results showing excellent agreement between data collected at 0.2 and 0.5 T. Species **6** and **7** show consistent coupling constants of $J \approx -6.0$ cm^{-1} and $g = 2.0$, in good agreement with literature values reported between 4 and 11 cm^{-1}.[23] Although the simulation of these data did not require the consideration of terms for paramagnetic impurities (TIP), the curves do not converge to $\mu_{eff} = 0$ as expected for strongly coupled systems. The residual effective moments of 0.68 and 0.85 μ_B for **6** and **7** are much smaller than the value of 1.73 μ_B for a single spin and can be solved by the inclusion of the intermolecular interaction term θ_{Weiss}. Whereas a small θ_{Weiss} contribution sufficed for **6**, a larger contribution was required for **7**. The nature of this intermolecular interaction can be explained by evaluation of the unit cells of **6** and **7**. In **6**, a short distance of ~3.3 Å is observed between vicinal molecules, but the aromatic rings are not parallel to one another. Molecules of **7**, on the other hand, display similar distances (3.36 Å between C11 and C21) along with nearly parallel aromatic rings, justifying the need for larger values of the θ_{Weiss} term. Furthermore, because fitting of the magnetization curve was performed with a simple dimeric model, the $5/2 \leftrightarrow 1/2$ equilibrium detected by EPR spectroscopic methods at low temperature may also contribute to the observed θ_{Weiss} behavior.

Computational Modeling. A series of electronic structure calculations were carried out on selected models aiming at

dx.doi.org/10.1021/ic2009368 |Inorg. Chem. 2011, 50, 8356–8366

Table 5. Isomer Energies

model compound	substituents -X; -R	geometry	relative energy[a] (kcal/mol)
archetypes			
$[Fe^{III}(L^{HH})_2]^+$	-H; -H	facial; cis	0.0
$[Fe^{III}(L^{HH})_2]^+$	-H; -H	meridional; cis	2.4
3	-H; -*tert*-butyl	facial; cis	0.0
3′	-H; -*tert*-butyl	meridional; cis	2.8
5	-H; -Cl	meridional; cis	0.0
5′	-H; -Cl	facial; cis	5.4
amphiphile			
$\mathbf{1}'^{meridional/cis}$	$-CH_3$; -H	meridional; cis	0.0
$\mathbf{1}'^{facial/cis}$	$-CH_3$; -H	facial; cis	6.6
$\mathbf{1}'^{facial/trans}$	$-CH_3$; -H	facial; trans	11.2
$\mathbf{1}''^{meridional/cis}$	$-CH_3$; -*tert*-butyl	meridional; cis	0.0
$\mathbf{1}''^{facial/cis}$	$-CH_3$; -*tert*-butyl	facial; cis	2.3

[a] B3LYP/6-31G(d).

comparing the experimentally observed geometric preferences for the archetypical species **3**−**7**, and at proposing an acceptable coordination model for the amphiphile **1**. The selected models include the previously published[4] $[Fe^{III}(L^{HH})_2]^+$, where L^{HH} indicates unsubstituted phenolates, the experimentally observed facial/cis **3**, and meridional/cis **5**, and their counterpart isomers meridional/cis **3′**, and facial/cis **5′**. All models consider $S = 5/2$, consistent with high-spin iron(III) species. The energy difference between these isomers was assessed and compared with the experimental structures. The models **3**, **3′**, **5**, and **5′** show good agreement with previous iron(III) amine complexes with cis-oriented phenolate rings. The unsubstituted $[Fe^{III}(L^{HH})_2]^+$ favors the facial isomer by ca. 2.4 kcal/mol against its meridional counterpart. However, as observed from the X-ray structures for complexes $\mathbf{5}\cdot CH_2Cl_2$ and **7**, the ligands are meridionally coordinated, thus suggesting that this trend is not suitable for halogen (-Cl, -Br, and -I)-substituted complexes. A summary of models and energies is presented in Table 5.

Complex **3** exhibiting a facial/cis coordination mode is favored by a small margin when compared to the meridional/cis isomer **3′**. This result is consistent with the $[Fe^{III}(L^{HH})_2]^+$ previously published.[4] On the other hand, the equivalent facial/cis mode adopted by **5′** is higher by 5.4 kcal/mol than the equivalent meridional/cis mode. This result suggests the meridional/cis isomer **5** as displaying the lowest-energy configuration, in excellent agreement with the obtained X-ray structure and UV−visible shifts. One can infer that the nature of the phenolate substituents leads to a given preferred isomer, although it is not completely clear at this point whether the driving force behind this selection is electronic or steric in nature. Similarly, the fairly low energy differences observed between isomers suggest that some extent of interconversion might occur in solution.

Having observed the structural, spectroscopic, and calculated differences between **3** and **5**, one can propose that the UV−visible band at ca. 540 nm observed for **1** relates to that at ca. 550 nm of **5**, rather than that with the expected 640 nm observed for **3**. Therefore, an acceptable coordination model for the amphiphile **1** was then searched. Model **1′**, with unsubstituted phenolates and a truncated methyl group replacing the original octadecyl chain, was used in order to streamline the calculations. Both facial/meridional and cis/trans configurations were

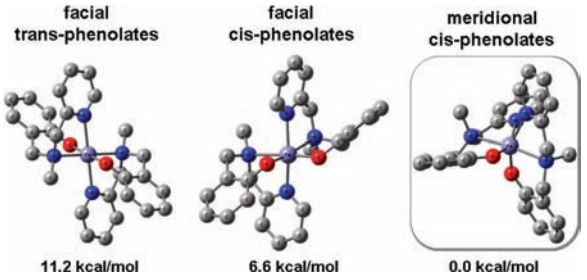

Figure 7. Model **1′** considering meridional/facial and cis/trans coordination modes.

modeled. The facial/trans mode represented by $\mathbf{1}'^{facial/trans}$ showed the highest relative energy at 11.2 kcal/mol, followed by the cis/facial configuration at 6.6 kcal/mol. The lowest-energy configuration obtained for **1′** was found to be meridional/cis, whereas the isomer meridional/trans failed to converge. Considering the consistency of the cis-phenolate arrangement in all isolated structures, one can suggest that—along with the UV−visible data—a preferred meridional/cis mode describes **1**. These results are shown in Figure 7. Inclusion of tertiary butyl groups on the phenolates was attempted in model **1″**. Comparable results favor the meridional/cis mode, although by a smaller margin similar to that for $[Fe^{III}(L^{HH})_2]^+$ and **3**. Considering the cis mode constant and observing the same phenolate substituents for **1** and **3**, it seems that a preferential meridional configuration is related to the presence of a more rigid tertiary amine.

CONCLUSIONS

In this study, we observed that iron(III) ions can form the monometallic **1** or a mixed mono- and bimetallic species **2** when coordinated to [NN′O] amphiphilic ligands. To investigate these trends, we have synthesized and studied the archetypes **3**−**9** that mimic the headgroups of such amphiphilic ligands. The preference for one of these nuclearities depends upon the nature of the solvent used for synthesis and the type of substituent in the phenol moiety. Methanol leads to monometallic species when *tert*-butyl-, methoxy-, and chloro-substituted ligands are used, whereas the bromo- and iodo-substituted ligands lead to bimetallic species bridged by methoxyde groups. When dichloromethane replaces methanol as the solvent, the same halogeno-substituted ligands yield monometallic species. Experimental and DFT data suggest that the halogeno-substituted species favor meridional coordination, in opposition to the facial coordination observed for *tert*-butyl- and methoxy-substituted compounds. Furthermore, the spectral features and EXAFS data for the iodo-substituted amphiphile **2** coincide with those of the iodo-substituted bimetallic compound, implying that the amphiphile also contains a bimetallic core. Interestingly, the spectral features of the *tert*-butyl-substituted amphiphile **1** relate better to the meridional/cis chloro-substituted species **5** than to the facial/cis *tert*-butyl archetype **3**. This suggests that the amphiphile displays a meridional/cis coordination mode. The DFT results support a small margin of preference for the meridional/cis coordination mode in the presence of less flexible tertiary amines on the ligand, as when a long alkyl chain is attached to the [NN′O] headgroup. On the basis of these results, the development of other iron(III)-containing amphiphiles in our group will consider (i) the use of dichloromethane, (ii) the avoidance of halogeno-substituted phenol moieties, and (iii) the presence of

dx.doi.org/10.1021/ic2009368 |*Inorg. Chem.* 2011, 50, 8356–8366

tertiary amines to target monometallic and redox-active precursors for LB films.

EXPERIMENTAL SECTION

General. All reagents were used as received from commercial sources, unless otherwise stated. Methanol was dried using calcium hydride, acetonitrile and dichloromethane were doubly purified using alumina columns in an Innovative Technologies solvent purification system. Infrared spectra were measured with 4000−400 cm^{-1} as KBr pellets on a Bruker Tensor FTIR spectrophotometer. The ^1H NMR spectra were measured using a Varian 400 MHz instrument. ESI (positive) spectra were measured in a Micromass Quattro LC triple quadrupole mass spectrometer, and experimental assignments were simulated for peak position and isotopic distribution. Elemental analyses were performed by Midwest Microlab (Indianapolis, Indiana). UV−visible spectra from 1.0×10^{-3} M and 1.0×10^{-4} M dichloromethane solutions were measured using a Cary 50 spectrophotometer in the range of 250−1100 nm. Cyclic voltammetry experiments were performed using a BAS 50W potentiometer. A standard three-electrode cell was employed with a glassy-carbon working electrode, a Pt-wire auxiliary electrode, and a Ag/AgCl reference electrode under an inert atmosphere at room temperature. Potentials were measured versus Ag/AgCl and presented versus Fc^+/Fc.[24] First-derivative X-band EPR spectra of the complexes were recorded at 77 K in dichloromethane frozen solutions (glass) using a Bruker ESP 300 spectrometer. Simulations of the iron(III) ion were performed with a program provided by Dr. Andrew Ozarowski, National High Magnetic Field Laboratory, Florida State University. Simulation of the low-spin $S = 1/2$ signals for the same ion was performed using a program developed by Prof. Bruce McGarvey. Variable-temperature magnetic susceptibility measurements were carried out with a Quantum Design MPMS XL-7 T SQUID magnetometer in the temperature range of 2−300 K under an applied magnetic field of 0.2 and 0.5 T. The powdered samples were filled in a gelatin capsule and fixed in a plastic straw. The measurement was carried out on a length of 4 cm, and 24 data points were taken. Experimental susceptibility data were corrected for diamagnetic contributions of the sample holder, and the underlying diamagnetism was corrected by using Pascal's constants. The program julX,[25] written by Dr. Eckhard Bill, Max Planck Institute for Bioinorganic Chemistry, was used for the simulation and analysis of magnetic susceptibility data.

Electronic Calculations. Spin-unrestricted density functional theory (DFT) calculations were carried out with the B3LYP[26] functional and the 6-31G(d)[27] basis set with the G03 version of Gaussian.[28] Geometries were fully optimized without symmetry constraints, and stationary points were verified via frequency analysis. Cartesian coordinates of all optimized structures are provided in the Supporting Information. All energies reported are the zero-point-corrected enthalpies.

EXAFS/XANES Spectroscopy. A sample of **2** was ground in Nujol to a final concentration of 5 mM and placed in aluminum sample holders between windows made from 1 mil Kapton tape. Data were recorded on beamline X3b at the National Synchrotron Light Source (Brookhaven National Laboratories, Upton, NY). The sample temperature was maintained at 25 K with a helium Displex closed-cycle cryostat, and fluorescence data were collected with a 13-element solid-state Ge detector. Total count-rates were maintained under 30 kHz with the use of a 6 μm Mn filter. All channels were inspected individually prior to data averaging, and a deadtime correction of 3 μs was applied, which had a negligible impact on the data. Data were collected in 5 eV steps in the pre-edge region (6912−7090 eV), 0.3 eV steps during the edge jump (7090−7139 eV), 2 eV steps in the near-edge region (7140−7410 eV), and 5 eV steps in the far-edge region (7410−k = 15.5 $Å^{-1}$). The reported spectrum represents the average of four data sets. The XANES and EXAFS data were analyzed using the software packages EXAFS123[29] and FEFF 8.4.[30] Best fits are reported based on simulation to the unfiltered EXAFS data. Although the data were recorded to k = 15.5 $Å^{-1}$, the EXAFS were analyzed to 14.3 $Å^{-1}$ due to noise at higher values of k.

X-ray Structural Determination for $5 \cdot CH_2Cl_2$, 6, 7, and $9 \cdot 2CHCl_3$. Diffraction data were collected on a Bruker APEX-II kappa geometry diffractometer with Mo−Kα radiation (λ = 0.71073 Å) and a graphite monochromator.[31] Frames were collected at 100 K as a series of sweeps with the detector at 40 mm and 0.3° between each frame. All structures were refined using Sheldrick's SHELX-97 software.[32] A summary of the crystal structure parameters for all four structures is contained in Table 6. Complex $5 \cdot CH_2Cl_2$ crystallized as dark rough flat rods. A sample of approximately $0.15 \times 0.4 \times 0.5$ mm^3 was used for the data collection. A total of 2120 frames were collected at 10 s/frame,

Table 6. Crystal Data for $5 \cdot CH_2Cl_2$, 6, 7 and $9 \cdot 2CHCl_3$

	$5 \cdot CH_2Cl_2$	6	7	$9 \cdot 2CHCl_3$
formula	$C_{27}H_{24}N_4O_6Cl_7Fe$	$C_{30}H_{34}N_4O_6Br_4Fe_2$	$C_{30}H_{34}N_4O_6I_4Fe_2$	$C_{28}H_{24}N_4O_6I_4FeCl_7$
fw	804.50	977.95	1165.91	1324.11
space group	$P2_1/c$	$P\bar{1}$	$P\bar{1}$	$P\bar{1}$
a (Å)	12.0275(5)	8.1851(12)	8.2018(3)	10.0197(3)
b (Å)	17.5329(6)	8.4501(13)	8.7957(3)	13.2289(3)
c (Å)	16.2589(6)	13.627(2)	13.8773(5)	16.1597(4)
α (deg)		86.442(5)	87.263(2)	103.7140(10)
β (deg)	106.180(2)	84.862(5)	85.849(2)	103.2290(10)
γ (deg)		64.000(5)	63.4580(10)	101.8180(10)
V ($Å^3$)	3292.8(2)	843.4(2)	893.12(6)	1948.19(9)
Z	4	1	1	2
temperature (K)	100(2)	100(2)	100(2)	100(2)
λ (Å)	0.71073	0.71073	0.71073	0.71073
ρ (g cm^{-3})	1.623	1.925	2.168	2.257
μ (mm^{-1})	1.073	5.646	4.315	4.082
$R(F)^a$ (%)	6.55	5.54	2.32	4.80
$R_w(F)^a$ (%)	12.08	13.58	5.24	12.50

^{a} $R(F) = \Sigma||F_o| - |F_c||/\Sigma|F_o|$; $R_w(F) = [\Sigma w(F_o^2 - F_c^2)^2/\Sigma w(F_o^2)^2]^{1/2}$.

dx.doi.org/10.1021/ic2009368 |Inorg. Chem. 2011, 50, 8356–8366

yielding 41 086 reflections, of which 8466 were independent. The hydrogen atoms were placed in observed positions. All non-hydrogen atoms were refined anisotropically. Complex **6** crystallized as red rods. A sample used for the data collection was approximately 0.2 × 0.04 × 0.04 mm^3. A total of 3011 frames were collected at 10 s/frame, yielding 16 396 reflections, of which 6142 were independent. Hydrogen positions were observed and refined. The dimeric molecule occupies a crystallographic inversion center. Complex **7** appeared as thin red flat rods, and a sample used for data collection was approximately 0.08 × 0.07 × 0.02 mm^3. A total of 3050 frames were collected at 15 s/frame, yielding 18 002 reflections, of which 5625 were independent. Hydrogen positions were placed in observed positions and refined. The dimeric molecule occupies a crystallographic inversion center. Complex **9**·2$CHCl_3$ crystallized as dark rods, and a sample 0.16 × 0.08 × 0.08 mm^3 was used for data collection. A total of 3791 frames were collected at 10 s/frame, yielding 38 493 reflections, of which 11351 were independent. Hydrogen positions were placed in calculated or observed positions. The asymmetric unit contains one cation, one anion, and two $CHCl_3$ solvent molecules.

Synthesis of the Ligands. The amphiphilic ligands $HL^{I\text{-}ODA}$ and $HL^{tBu\text{-}ODA}$ and a series of the archetypical HL^{RA} ligands (R = methoxy, chloro, bromo, and iodo) were synthesized as reported in the literature.[1,2]

Synthesis of the Complexes. *Amphiphiles* $[Fe^{III}(L^{tBu\text{-}ODA})_2]ClO_4$ (**1**) *and* $[\{Fe^{III}(L^{I\text{-}ODA})(OCH_3)(\mu\text{-}OCH_3)\}_2]$ (**2**). A solution of the appropriate ligand (1.0 mmol) and Et_3N (0.28 mL, 2.0 mmol) was prepared in 20 mL of a 1:1 MeOH/CH_2Cl_2 solvent mixture. This solution was then added dropwise to a 5 mL methanol solution of $[Fe^{III}(H_2O)_6](ClO_4)_3$ (0.258 g, 0.5 mmol) in a round-bottom flask. After the ligand/Et_3N solution had been added, it was heated at 50 °C for 2 h. A dark solution formed, from which the solvent was rotoevaporated. The resulting waxy product was washed with water and cold methanol, extracted with dichloromethane, and dried in vacuum.

$[Fe^{III}(L^{tBu\text{-}ODA})_2]ClO_4$ (**1**). Yield = 0.39 g (65%). IR (KBr, cm^{-1}): 1608 (m), 1572 (m), 1465 (s) (C═Npy, C═CAr), 1267 (s) (C−O), 1098 (uncoordinated ClO_4^-). ESI pos. in MeOH: m/z = 1210.6 for $[Fe^{III}(L^{tBu\text{-}ODA})_2]^+$.

$[\{Fe^{III}(L^{I\text{-}ODA})(OCH_3)(\mu\text{-}OCH_3)\}_2]$ (**2**). Yield = 0.47 g (60%). IR (KBr, cm^{-1}): 1610 (m), 1566 (m), 1436 (s) (C═Npy, C═CAr), 1309 (s) (C−O). ESI pos. in MeOH: m/z = 1638.6 $[M - (OCH_3)]^+$, 1593.2 $[M - 2(OCH_3)\text{-}CH_3]^+$

Archetypical Complexes $[Fe^{III}(L^{tBu\text{-}A})_2]ClO_4$ (**3**), $[Fe^{III}(L^{OMe\text{-}A})_2]ClO_4$ (**4**), *and* $[Fe^{III}(L^{Cl\text{-}A})_2]ClO_4$ (**5**·*MeOH*) *in Methanol.* To a 30 mL methanol solution containing the appropriate ligand (2.0 mmol) and Et_3N (0.28 mL, 2.0 mmol), a 5 mL methanol solution of $[Fe^{III}(H_2O)_6](ClO_4)_3$ (0.46 g, 1.0 mmol) was added dropwise. The resulting solution was heated at 50 °C for 1 h and then cooled to room temperature. A microcrystalline precipitate formed and was filtered and washed with cold methanol. The solid was isolated and dried under vacuum.

$[Fe^{III}(L^{OMe\text{-}A})_2]ClO_4$ (**4**). Yield = 0.51 g (80%). IR (KBr, cm^{-1}): 1608 (m), 1571 (m), 1458 (s) (C═Npy, C═CAr), 1250 (s) (C−O), 1121−1092 (free ClO_4^-). Elemental Anal. Calcd for $[C_{28}H_{30}Cl_1N_4O_8Fe_1]$: C, 52.39; H, 4.71; N, 8.73. Found: C, 51.97; H, 4.63; N, 8.44. ESI pos. in MeOH: m/z = 542.1 for $[Fe^{III}(L^{OMe\text{-}A})_2]^+$.

$[Fe^{III}(L^{Cl\text{-}A})_2]ClO_4$ (**5**·*MeOH*). Yield = 0.58 g (82%). IR (KBr, cm^{-1}): 1609 (m), 1571 (m), 1450(s) (C═Npy, C═CAr), 1286 (m) (C−O), 1121−1090 (free ClO_4). Elemental Anal. Calcd for $[C_{27}H_{26}Cl_5N_4O_7Fe_1]$: C, 43.14; H, 3.49; N, 7.45. Found: C, 43.02; H, 3.81; N, 7.10. ESI pos. in MeOH: m/z = 617.9 for $[Fe^{III}(L^{Cl\text{-}A})_2]^+$. Recrystallization of **5** MeOH in 1:1 MeOH/CH_2Cl_2 yielded X-ray quality crystals of **5** CH_2Cl_2 that exhibit identical spectroscopic features.

Complexes $[\{Fe^{III}(L^{Br\text{-}A})(OCH_3)(\mu OCH_3)\}_2]$(**6**) *and* $[\{Fe^{III}(L^{I\text{-}A})(OCH_3)(\mu\text{-}OCH_3)\}_2]$ (**7**) *in Methanol.* A 5 mL methanol solution of $[Fe^{III}(H_2O)_6](ClO_4)_3$ (0.46 g, 1.0 mmol) was added dropwise to a 30 mL methanol solution containing the appropriate ligand (1.0 mmol) and Et_3N (0.14 mL, 1.0 mmol). The resulting solution was heated at 50 °C for 1 h and then cooled to room temperature. A dark-colored precipitate formed, was filtered, and washed with cold methanol. A microcrystalline solid was isolated and dried under vacuum.

$[\{Fe^{III}(L^{Br\text{-}A})(OCH_3)(\mu\text{-}OCH_3)\}_2]$ (**6**). Yield = 0.77 g (80%). IR (KBr, cm^{-1}): 1606 (m), 1573 (m), 1445 (s) (C═N py,C═CAr),1313 (m) (C−O). Elemental Anal. Calcd for $[C_{30}H_{34}N_4O_6Br_4Fe_2]$: C, 36.85; H, 3.50; N, 5.73. Found: C, 36.74; H, 3.66; N, 5.53. ESI pos. in MeOH: m/z = 942.8 $[M - OCH_3]^+$, 912.8 $[M - 2(OCH_3)H]^+$.

$[\{Fe^{III}(L^{I\text{-}A})(OCH_3)(\mu\text{-}OCH_3)\}_2]$ (**7**). Yield = 0.87 g (75%). IR (KBr, cm^{-1}): 1606 (m), 1564 (m), 1443 (s) (C═N Py,C═CAr), 1309 (m) (C−O). Elemental Anal. Calcd for $[C_{30}H_{34}Fe_2N_4O_6I_4]$: C, 30.90; H, 2.94; N, 4.81. Found: C, 31.08; H, 3.05; N, 4.61. ESI pos. in MeOH: m/z = 1134.9 $[M - OCH_3]^+$, 1102.8 $[M - 2(OCH_3)H]^+$.

Complexes $[Fe^{III}(L^{Br\text{-}A})_2]ClO_4$ (**8**) *and* $[Fe^{III}(L^{I\text{-}A})_2]ClO_4$ (**9**·CH_2Cl_2·H_2O) *in Dichloromethane.* A 2 mL acetonitrile solution of $[Fe^{III}(H_2O)_6](ClO_4)_3$ (0.46 g, 1.0 mmol) was added to a 30 mL dichloromethane solution containing the appropriate ligand (2.0 mmol) and Et_3N (0.28 mL, 2.0 mmol). The resulting solution was heated at 30 °C for 1 h and then cooled to room temperature. A dark-blue precipitate formed upon slow evaporation of solvent, was filtered, and washed with water and then ether. An amorphous solid was isolated and dried under vacuum.

$[Fe^{III}(L^{Br\text{-}A})_2]ClO_4$ (**8**). Yield = 0.76 g (86%). IR (KBr, cm^{-1}): 1608 (m), 1575 (m), 1441 (s) (C═Npy, C═CAr), 1284 (m) (C−O), 1121−1090 (free ClO_4^-). Elemental Anal. Calcd for $[C_{26}H_{22}ClBr_4FeN_4O_6Fe_1]$: C, 34.80; H, 2.47; N, 6.24. Found: C, 35.09; H, 2.57; N, 6.03. ESI pos. in MeOH: m/z = 793.7 for $[Fe^{III}(L^{Br\text{-}A})_2]^+$.

$[Fe^{III}(L^{I\text{-}A})_2]ClO_4$ (**9**·CH_2Cl_2·H_2O). Yield = 0.91 g (84%). IR (KBr, cm^{-1}): 1592 (m), 1570 (m), 1433 (s) (C═Npy, C═CAr), 1281 (m) (C−O), 1108−1089 (free ClO_4^-). Elemental Anal. Calcd for $[C_{27}H_{26}Cl_3I_4FeN_4O_7]$: C, 27.29; H, 2.21; N, 4.71. Found: C, 26.85; H, 2.14; N, 4.60. ESI pos. in MeOH: m/z = 985.7 for $[Fe^{III}(L^{I\text{-}A})_2]^+$. Recrystallization of **9**·CH_2Cl_2·H_2O in 1:1 MeOH/$CHCl_3$ yielded X-ray quality crystals of **9**·2$CHCl_3$ that exhibit identical spectroscopic features.

■ ASSOCIATED CONTENT

Supporting Information. XAS spectrum, ORTEP drawing for the molecular structure of **6**, temperature-dependent measurement of the magnetic moment for **7**, Cartesian coordinates for DFT calculations, and crystallographic file. This material is available free of charge via the Internet at http://pubs.acs.org.

■ AUTHOR INFORMATION

Corresponding Author
*E-mail: cnverani@chem.wayne.edu.

■ ACKNOWLEDGMENT

C.N.V. thankfully acknowledges support from the National Science Foundation (Grants CHE-0718470 and CHE-1012413). The authors thank Dr. Lew Hryhorczuk of the WSU-Central Instrument Facility for the measurement of the mass spectra. One of the reviewers is also acknowledged for insightful comments.

■ REFERENCES

(1) Shakya, R.; Imbert, C.; Hratchian, H. P.; Lanznaster, M.; Heeg, M. J.; McGarvey, B. R.; Allard, M.; Schlegel, H. B.; Verani, C. N. *Dalton Trans.* **2006**, 2517.

(2) Lesh, F. D.; Hindo, S. S.; Heeg, M. J.; Allard, M. M.; Jain, P.; Peng, B.; Hryhorczuk, L.; Verani, C. N. *Eur. J. Inorg. Chem.* **2009**, 345.

(3) (a) Lim, N. C.; Ewart, C. B.; Bowen, M. L.; Ferreira, C. L.; Barta, C. A.; Adam, M. J.; Orvig, C. *Inorg. Chem.* **2008**, *47*, 1337. (b) Sarkar, S.; Mondal, A.; Chopra, D.; Ribas, J.; Rajak, K. K. *Eur. J. Inorg. Chem.* **2006**, *17*, 3510. (c) Biswas, S.; Mitra, K.; Chattopadhyay, S. K.; Adhikary, B.; Lucas, C. R. *Transition Met. Chem.* **2005**, *30*, 393. (d) Motoyama, T.; Shimazaki, Y.; Yajima, T.; Nakabayashi, Y.; Naruta, Y.; Yamauchi, O. *J. Am. Chem. Soc.* **2004**, *126*, 7378. (e) Mondal, A.; Sarkar, S.; Chopra, D.; Row, T. N.; Rajak, K. K. *Dalton Trans.* **2004**, 3244. (f) Drechsel, S. M.; Kaminski, R.; Nakagaki, S.; Wypych, F. *J. Colloid Interface Sci.* **2004**, *277*, 138. (g) Baruah, B.; Das, S.; Chakravorty, A. *Inorg. Chem.* **2002**, *41*, 4502. (h) Cameron, P. A.; Gibson, V. C.; Redshaw, C.; Segal, J. A.; Bruce, M. D.; White, A. J. P.; William, D. J. *Chem. Commun.* **1999**, 1883. (i) Neves, A.; Verani, C. N.; Brito, M. A.; Vencato, I.; Mangrich, A.; Oliva, G.; Dulce, D. H.; Souza., F.; Batista, A. A. *Inorg. Chim. Acta* **1999**, *290*, 207. (j) Hatfield, W. E.; Bunger, F. L. *Inorg. Chem.* **1969**, *08*, 1194.

(4) Imbert, C.; Hratchian, H. P.; Lanznaster, M.; Heeg, M. J.; Hryhorczuk, L. M.; McGarvey, B. R.; Schlegel, H. B.; Verani, C. N. *Inorg. Chem.* **2005**, *44*, 7414.

(5) Shakya, R.; Hindo, S. S.; Wu, L.; Allard, M. M.; Heeg, M. J.; Hratchian, H. P.; McGarvey, B. R.; da Rocha, S. R. P.; Verani, C. N. *Inorg. Chem.* **2007**, *46*, 9808.

(6) (a) Randall, C. R.; Shu, L.; Chiou, Y.-M.; Kagen, K. S.; Ito, M.; Kitajima, N.; Lachicotte, R. J.; Zang, Y.; Que, L., Jr. *Inorg. Chem.* **1985**, *34*, 1036. (b) Roe, A. L.; Schneider, D. J.; Mayer, R. J.; Pyrz, J. W.; Widom, J.; Que, L., Jr. *J. Am. Chem. Soc.* **1984**, *106*, 1676.

(7) The notation <A_1B_2> indicates that A is trans to B, and subscripts 1 and 2 designate, respectively, the first and the second ligand. Adapted by: (a) Miessler, G.; Tarr, D. *Inorganic Chemistry*; Pearson-Prentice Hall: Upper Saddle River, NJ, 2004; pp 311−315 from (b) Bailar, J., Jr. *J. Chem. Educ.* **1957**, *34*, 334−338 and 623−626.

(8) (a) Mayilmurugan, R.; Visvaganesan, K.; Suresh, E.; Palaniandavar, M. *Inorg. Chem.* **2009**, *48*, 8771. (b) Viswanathan, R.; Palaniandavar, M.; Balasubramanian, T.; Muthiah, T. P. *J. Chem. Soc., Dalton Trans.* **1996**, 2519. (c) Viswanathan, R.; Palaniandavar, M. *J. Chem. Soc., Dalton Trans.* **1995**, 1259.

(9) (a) Shakya, R.; Powell, D. R.; Houser, R. P. *Eur. J. Inorg. Chem.* **2009**, 5319. (b) Walker, J. D.; Poli, R. *Inorg. Chem.* **1990**, *29*, 756. (c) Krebs, B.; Schepers, K.; Bremer, B.; Henkel, G.; Althaus, E.; Muller-Warmuth, W.; Griessar, K.; Haase, W. *Inorg. Chem.* **1994**, *33*, 1907.

(10) Shongwe, M. S.; Kaschula, C. H.; Adsetts, M. S.; Ainscough, E. W.; Brodie, A. M.; Morris, M. J. *Inorg. Chem.* **2005**, *44*, 3070.

(11) Viswanathan, R.; Palaniandavar, M.; Prabakaran, P.; Muthiah, P. T. *Inorg. Chem.* **1998**, *37*, 3881.

(12) Thich, J. A.; Chih Ou, C.; Powers, D.; Vasiliou, B.; Masteropalo, D.; Potenza, J. A.; Schugar, H. J. *J. Am. Chem. Soc.* **1976**, *98*, 145.

(13) (a) Davis, M. I.; Orville, A. M.; Neese, F.; Zaleski, J. M.; Lipscomb, J. D.; Solomon, E. I. *J. Am. Chem. Soc.* **2002**, *124*, 602. (b) Gaber, B. P.; Miskowski, V.; Spiro, T. G. *J. Am. Chem. Soc.* **1974**, *96*, 6868.

(14) Banse, F.; Balland, V.; Philouze, C.; Riviere, E.; Tchertanova, L.; Giererd, J. *Inorg. Chim. Acta* **2003**, *353*, 223.

(15) (a) Keenan, S. L.; Peterson, K. P.; Peterson, K.; Jacobson, K. *J. Chem. Educ.* **2008**, *85*, 558. (b) Hammett, L. P. *J. Am. Chem. Soc.* **1937**, *59*, 96.

(16) Shongwe, M. S.; Al-Rashdi, B. A.; Adams, H.; Morris, M. J.; Mikuriya, M.; Hearne, G. R. *Inorg. Chem.* **2007**, *46*, 9558.

(17) Tang, J.; Costa, J. S.; Smulders, S.; Molnár, G.; Bousseksou, A.; Teat, S. J.; Li, Y.; van Albada, G. A.; Gamez, P.; Reedijk, J. *Inorg. Chem.* **2009**, *48*, 2128.

(18) Sim, G. P.; Sinn, E.; Petty, R. H.; Merrill, C. L.; Wilson, L. J. *Inorg. Chem.* **1981**, *20*, 1213.

(19) Mabbs, F. E.; Collison, D. *Electron Paramegnetic Resonance of d Transition Metal Compounds*; Elsevier: Amsterdam, 1992.

(20) A total of 16 simulations were attempted involving the spin Hamiltonian $H = \beta_e \hat{S} \cdot g \cdot B + D[\hat{S}_Z^2 - (35/12)] + E[\hat{S}_x^2 - \hat{S}_y^2]$ and the zero-field parameters D, E, B_4^0, B_4^2, and B_4^4 allowed for $S = 5/2$, with $g = 2.00$. As mentioned above, the main peak at $g \sim 4.3$ occurs only when $|D| \gg h\nu$ and $|E|$ is close to $|D/3|$. When $E = 0$, the main peak is near $g = 6$. For other values of E, there are often three peaks. Simulations used $D = 3000$ and 9000 G and probed E values close to $D/3$ with $B_4^0 \neq 0$ and $B_4^2 = B_4^4 = 0$.

(21) (a) McGarvey, B. R. *Coord. Chem. Rev.* **1998**, *170*, 75. (b) McGarvey, B. R. *Quim. Nova* **1998**, *21*, 206.

(22) Thus, z is perpendicular to the xy MO, y to the xz MO, etc.

(23) (a) Horn, A., Jr.; Vencato, I.; Bortoluzzi, A. J.; Hörner, R.; Nome Silva, R. A.; Spoganicz, B.; Drago, V.; Terenzi, H.; de Oliveira, M. C. B.; Werner, R.; Haase, W.; Neves, A. *Inorg. Chim. Acta* **2005**, *358*, 339. (b) Houjou, H.; Kanesato, M.; Hiratani, K.; Mandon, D. *Chem.—Eur. J.* **2004**, *10*, 4576. (c) Scarpellini, M.; Neves, A.; Bortoluzzi, A. J.; Vencato, I.; Drago, V.; Ortiz, W. A.; Zucco, C. *J. Chem. Soc., Dalton Trans.* **2001**, 2616.(d) Gall, F. L.; Biani, F. F.; Caneschi, A.; Cinelli, P.; Cornia, A.; Fabretti, A. C.; Gatteschi, D. *Inorg. Chim. Acta.* **1997**, *262*, 123.

(24) Gagne, R.; Koval, C.; Licenski, G. *Inorg. Chem.* **1980**, 2854.

(25) http://ewww.mpi-muelheim.mpg.de/bac/logins/bill/julX_en.php.

(26) (a) Becke, A. D. *J. Chem. Phys.* **1993**, *98*, 5648. (b) Lee, C.; Yang, W.; Parr, R. G. *Phys. Rev. B* **1988**, *37*, 785. (c) Miehlich, B.; Savin, A.; Stoll, H.; Preuss, H. *Chem. Phys. Lett.* **1989**, *157*, 200.

(27) (a) Binning, R. C., Jr.; Curtiss, L. A. *J. Comput. Chem.* **1990**, *11*, 1206. (b) Blaudeau, J.-P.; McGrath, M. P.; Curtiss, L. A.; Radom, L. *J. Chem. Phys.* **1997**, *107*, 5016. (c) Ditchfield, R.; Hehre, W. J.; Pople, J. A. *J. Chem. Phys.* **1971**, *54*, 724. (d) Francl, M. M.; Pietro, W. J.; Hehre, W. J.; Binkley, J. S.; DeFrees, D. J.; Pople, J. A.; Gordon, M. S. *J. Chem. Phys.* **1982**, *77*, 3654. (e) Gordon, M. S. *Chem. Phys. Lett.* **1980**, *76*, 163. (f) Hariharan, P. C.; Pople, J. A. *Theor. Chem. Acc.* **1973**, *28*, 213. (g) Hariharan, P. C.; Pople, J. A. *Mol. Phys.* **1974**, *27*, 209. (h) Hehre, W. J.; Ditchfield, R.; Pople, J. A. *J. Chem. Phys.* **1972**, *56*, 2257. (i) Rassolov, V. A.; Pople, J. A.; Ratner, M. A.; Windus, T. L. *J. Chem. Phys.* **1998**, *109*, 1223. (j) Rassolov, V. A.; Ratner, M. A.; Pople, J. A.; Redfern, P. C.; Curtiss, L. A. *J. Comput. Chem.* **2001**, *22*, 976.

(28) Frisch, M. J.; Trucks, G. W.; Schlegel, H. B.; Scuseria, G. E.; Robb, M. A.; Cheeseman, J. R.; Montgomery, J. A., Jr.; Vreven, T.; Kudin, K. N.; Burant, J. C.; Millam, J. M.; Iyengar, S. S.; Tomasi, J.; Barone,V.; Mennucci, B.; Cossi, M.; Scalmani, G.; Rega, N.; Petersson, G. A.; Nakatsuji, H.; Hada, M.; Ehara, M.; Toyota, K.; Fukuda, R.; Hasegawa, J.; Ishida, M.; Nakajima, T.; Honda, Y.; Kitao, O.; Nakai, H.; Klene, M.; Li, X.; Knox, J. E.; Hratchian, H. P.; Cross, J. B.; Bakken, V.; Adamo, C.; Jaramillo, J.; Gomperts, R.; Stratmann, R. E.; Yazyev, O.; Ayala, P.; Morokuma, Y. K.; Voth, G. A.; Salvador, P.; Dannenberg, J. J.; Zakrzewski, V. G.; Dapprich, S.; Daniels, A. D.; Strain, M. C.; Farkas, O.; Malick, D. K.; Rabuck, A. D.; Raghavachari, K.; Foresman, J. B.; Ortiz, J. V.; Cui, Q.; Baboul, A. G.; Clifford, S.; Cioslowski, J.; Stefanov, B. B.; Liu, G.; Liashenko, A.; Piskorz, P.; Komaromi, I.; Martin, R. L.; Fox, D. J.; Keith, T.; Al-Laham, M. A.; Peng, C. Y.; Nanayakkara, A.; Challacombe, M. P.; Gill, M. W.; Johnson, B.; Chen, W.; Wong, M. W.; Gonzalez, C.; Pople, J. A. *Gaussian 03*, revision D.01; Gaussian, Inc.: Wallingford, CT, 2004.

(29) Scarrow, R. C.; Shearer, J. *EXAFS123*, v.0.10; University of Nevada, Reno: Reno, NV, 2010.

(30) (a) Ankudinov, A. L.; Ravel, B.; Rehr, J. J.; Conradson, S. D. *Phys. Rev. B: Condens. Matter Mater. Phys.* **1998**, *58*, 7565. (b) Ankudinov, A. L.; Bouldin, C. E.; Rehr, J. J.; Sims, J.; Hung, H. *Phys. Rev. B: Condens. Matter Mater. Phys.* **2002**, *65*, 104107/1.

(31) APEX II collection and processing programs are distributed by the manufacturer, Bruker AXS Inc., Madison, WI.

(32) Sheldrick, G. *SHELX-97*; University of Gottingen: Gottingen, Germany, 1997.